Creating group-level functionally-defined atlases for diagnostic classification

Francisco Pereira*, Jennifer M. Walz†, Ertan Cetingul *, Sandra Sudarsky*, Mariappan Nadar*, Ruchika Prakash‡
*Imaging and Computer Vision, Siemens Corporation, Corporate Technology
755 College Road E, Princeton NJ 08540
francisco-pereira@siemens.com
†Department of Biomedical Engineering, Columbia University
‡Department of Psychology, Ohio State University

***Abstract*—In this paper we introduce a method to produce a subdivision of an anatomical atlas by taking into account the similarity of resting state functional MRI time series within anatomically-defined regions of interest. This method differs from others in that the resulting atlases are comparable across subjects, making group analyses possible. Finally, we show that the functional connectivity matrices obtained with this method can be used in a diagnostic classification task and that they enhance a classifier's ability to extract relevant information from the data, leading to more interpretable prediction models in the process.**

I. Introduction

Functional connectivity features have been used in multiple diagnostic classification settings (e.g. Multiple Sclerosis [1] or ADHD [2]). They are typically obtained by using an atlas to partition the brain into regions of interest (ROIs), computing the average time series in a resting state fMRI (rs-fMRI) dataset for all the voxels in each ROI and deriving a $\#\text{ROIs} \times \#\text{ROIs}$ *functional connectivity* matrix. The atlas plays two roles in this process: aggregating multiple time series and reducing the data from each subject to a format that can be compared across subjects.

The division of the brain is driven by anatomical and/or histological concerns, in general, not functional activation or the presence of structural connections between regions of interest. Furthermore, each ROI is often large and, therefore, its functional activation during resting state or performance of a task could be quite heterogeneous.

These issues can affect functional connectivity measurements between a pair of ROIs. First, the notion of an "average" time series for a ROI is dubious if what is being averaged are voxels engaged in processes with different time series of activation. We could, for instance, have a portion of an ROI A correlated with region B exclusively, another with C exclusively, and the average of those portions would be less correlated with B or C than each portion was in reality. Conversely, knowing correlations are absent, rather than partial, could be particularly useful for diagnostic classification.

These concerns have led to the idea of producing *individualized* atlases where anatomical ROIs are divided into *functionally homogeneous* parcels. This idea has been explored by various groups, e.g. [3] proposes the use of spectral clustering of rs-fMRI series, constrained by spatial adjacency, to generate a finer grain atlas, and [4] uses short-TR rs-fMRI and a notion of "stable seed" to grow a large of number of regions that are then aggregated using spatially constrained hierarchical clustering. Our work also entails the production of individualized atlases, albeit using *modularity* [5] over a neighbourhood graph for clustering voxels.

Our work differs from these in that we also propose a simple approach – and extensions thereof – to make the resulting individualized atlases *correspond across subjects*. Furthermore, we validate this approach by showing that it leads to sparser, fine-grained functional connectivity matrices that allow for increased classification accuracy, despite containing an order of magnitude more features than would be obtained using the AAL atlas, and a more interpretable classifier overall.

II. Data

Structural [1] and resting state functional [2] data were collected at Ohio State University. The dataset underwent standard preprocessing using FSL [6] and was then detrended, temporally filtered ($0.009\text{Hz} < f < 0.08\text{Hz}$) and spatially smoothed (all steps as in [2]). The structural image of each subject was registered to the MNI template using *fnirt*. After excluding subjects who moved excessively, there were 26 healthy controls and 46 MS patients.

III. Our method

The end result of this algorithm is a version of a source atlas where all the ROIs have been divided into a data-driven number of parcels that are functionally homogeneous to a degree, yielding the same number of parcels in each subject.

A. Within-subject steps

1) register structural image to MNI template
2) mask the AAL atlas [7] with it to create a subject-specific version

[1]Structural data: MPRAGE, 160 contiguous sagittal slices (TE/TR/TE 3.7/8.1/1005 ms) collected in an ascending fashion parallel to the AC-PC and using a spoiled gradient sequence (240x240 mm FOV; 1 mm thick slices, with a $1 \times 1 \times 1$ in-plane resolution) with a flip angle of 8 degrees.

[2]Resting state data: eyes open, T2*-weighted echo planar images (EPIs) collected with TR/TE 2000/24 ms, flip angle=80 degrees, 37 slices, 3.44mm isotropic voxel size, 180 volumes.

3) use same transformation to place functional data in template space

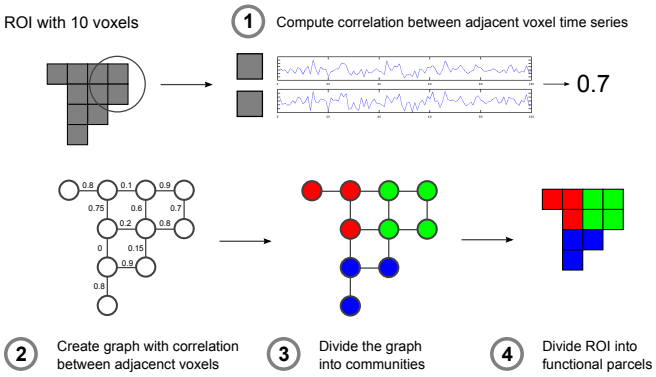

Figure 1. Division of a ROI into functional parcels.

We then segment each ROI into parcels whose voxels have similar time series of activation in the resting state functional data (Figure 1):

1) For each pair of spatially adjacent voxels i and j in the ROI (j lies anywhere in the 26-voxel cuboid around i), compute the correlation between the time series of voxel i and voxel j in the resting state dataset.
2) Create a graph with one node per voxel, with an edge between any adjacent voxels i and j. Label the edge with a weight equal to the correlation between their time series or 0, if that correlation is negative.
3) Use modularity to split this graph into *communities*, subsets that are more closely connected to each other than to the rest of the graph (with code from [5]).
4) The communities identified are sets of spatially contiguous voxels and become the parcels into which the ROI is subdivided.

Note that, at this stage of the algorithm, each ROI might have a different number of parcels, depending on how many subsets of highly correlated adjacent voxels it contains; the number of parcels is determined automatically by the modularity code, with no parameters to set.

B. Group-level steps

The second stage of the algorithm takes the subject-specific atlases and the functionally-driven parcellations of each ROI, and uses them to create a new, group-level parcellation where 1) each ROI has the same number of parcels across *all* subjects and 2) there is an established correspondence between parcels inside the ROI. The algorithm starts with subject-specific atlases, restricted to voxels present in all subjects.

1) Equalize the number of parcels in each ROI across all subjects: For each ROI, we determine the minimum number of parcels m that that ROI was divided into across all the subjects being considered. For each subject, we re-cluster the voxels in that ROI to yield m parcels. We do this by identifying the smallest parcel and joining it to the smallest of its *adjacent* parcels; this process is iterated until there are exactly m parcels.

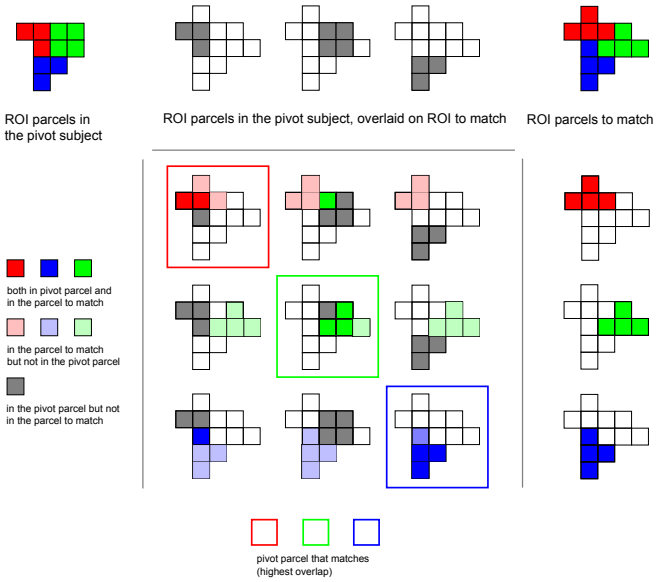

Figure 2. Matching the ROI parcels in one of the subjects with the ROI parcels in a pivot subject.

2) Establish a correspondence between the parcels: We use a greedy algorithm to establish a correspondence between the parcels of an ROI across subjects, illustrated in Figure 2 for a 3-parcel ROI:

1) Identify a *pivot subject*, one with the least difference between the numbers of voxels in the largest and smallest parcels; the goal is to minimize the chance of having small parcels, as these are not good targets for matching.
2) For each subject, find the bipartite matching between the ROI parcels in the pivot subject (top left corner of Figure 2) and the parcels in its ROI (top right corner of Figure 2):
   a) compute the spatial overlap fractions [3] between each of the parcels to match (right of Figure 2) and the parcels in the pivot subject (top of Figure 2); the 3×3 overlaps are depicted in the center of Figure 2
   b) match the parcels with the greatest spatial overlap, eliminate those from consideration, repeat until all parcels have been matched
3) For each subject, renumber the parcels of the ROI so that the parcels are in the same order as those in the pivot subject.

The result, in each subject, is the desired individualized atlas where parcels contain voxels with homogeneous time series

[3] Overlap is $\frac{\#\text{both}}{\#\text{both}+\#\text{xor}}$, where $\#both$ is the number of voxels in both, $\#xor$ is the number of voxels in one but not the other.

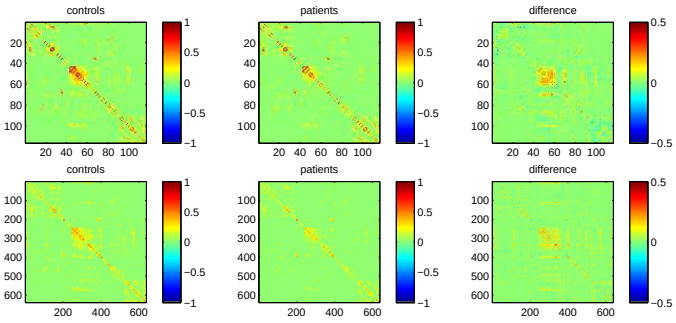

Figure 3. **top:** the average matrices for controls and patients, as well as their difference, using the AAL atlas **bottom:** same using the subdivided AAL atlas

and parcels correspond across all the subjects in the group.

The process could be refined by using a more elaborate function to score the matching between two parcels. One possibility would be to aggregate spatial overlap, as described above, and also a *functional connectivity profile* of the parcel with respect to all other ROIs in the original atlas for that subject. This profile consists of the correlations between the average time series of voxels in the parcel and the average time series of all other ROIs in the brain; the rationale is that two parcels correspond better – functionally – if they display similar patterns of correlation (or lack thereof) to other regions.

IV. Experiments

A. Datasets

Using our method with the AAL atlas as a starting point (116 ROIs) we obtained subject-specific atlases with 639 ROIs; we then used each atlas to produce functional connectivity matrices for each subject, as follows. We calculated the average rs-fMRI time series of all voxels in each ROI and then the correlation between all pairs of ROIs, yielding a correlation matrix. We applied a Fisher z-transformation to each matrix entry and tested the null hypothesis that the corresponding correlation was 0. The resulting matrix of p-values was thresholded using False Discovery Rate [8] ($q = 0.05$) and entries were kept if their corresponding p-value was significant, or 0 otherwise. Figure 3 shows the average matrices for controls and patients, as well as the differences between them, using the 116 and 639 ROI atlases.

Given the matrix for a subject, the entries for each distinct ROI pair became *features*, yielding an *example* vector. This was done for every patient and control, and their respective example vectors (and labels) became a dataset on which to train and test a diagnostic classifier. The raw datasets had 6670 and 203841 features for the 116 and 639 ROI atlases, respectively. Each feature that had a constant value across all subjects – 0, typically – was eliminated, and thus the final datasets had 4073 and 125967 features. Henceforth we will refer to the datasets as AAL and AALsub.

Table II
Top 10 high-impact ROIs, using the original (116 ROIs) and subdivided (639 ROIs, P# is the parcel) atlases.

AAL (116)	impact	AALsub (639)	impact
Paracentral_Lobule_R	0.125	Postcentral_L_P2_L	0.088
Occipital_Mid_L	0.085	Paracentral_Lobule_R_P4_R	0.069
Postcentral_L	0.060	Postcentral_R_P2_R	0.047
Postcentral_R	0.059	Postcentral_R_P3_R	0.042
Temporal_Inf_R	0.053	Occipital_Mid_L_P4_L	0.042
Parietal_Sup_R	0.045	Cingulum_Ant_R_P2_R	0.042
Temporal_Pole_Mid_L	0.044	Postcentral_R_P1_R	0.039
Occipital_Inf_R	0.042	Cingulum_Ant_L_P2_L	0.038
Occipital_Sup_L	0.041	Occipital_Inf_L_P2_L	0.032
Cerebelum_8_R	0.040	Precuneus_L_P1_L	0.031

B. Classification

We ran classification experiments for the AAL and AALsub datasets. We used a linear SVM [9] with default parameters to make the prediction, in a leave-one-subject-of-each-class-out cross-validation, with classes being "patients" and "controls" [10]. We selected features in the training set of each fold, using a t-test to score each feature; the number of features used was determined by *nested* cross-validation inside the training set, trying out 10, 25, 50, 100, 250, 500, 1000, 1500, 2000, 2500, 3000 or all features and selecting the number leading to the best result (different from fold to fold) [4]. In Table I we report results using the number of features determined through nested cross-validation (#nested), as well as using each fixed number of features, for comparison.

The measure of success used was classification accuracy, i.e. the fraction of subjects whose diagnostic label was predicted correctly when it was left out in cross-validation. In order to maintain a balanced dataset, we sampled 26 patients from the 46 available and ran the cross-validation procedure in the resulting 52 example dataset. This was done 30 times, sampling a different subset each time, and the results reported were the average across those 30 samplings. The nested cross-validation results were significantly better than chance for either AAL or AALsub, and accuracy higher for AALsub. Finally, and so as to exclude motion confounds, we attempted to classify the two groups based on median or maximum values across time of each subject's 6 motion correction parameters; the results were not above chance.

C. ROI impact

We determined the *impact* of each ROI in providing the information used by the classifier when successful [5]. For a particular training and test set, the impact of each *feature*

[4]Note that in AALsub feature selection operates on two orders of magnitude more features than in AAL.

[5]We did this for the models obtained by using nested cross-validation to select the number of features in each fold, so as not to pick a model that was better by chance.

Table I
CLASSIFICATION ACCURACY RESULTS USING ORIGINAL AAL ATLAS (116 ROIS) AND THE SUBDIVIDED AAL ATLAS (639 ROIS). CLASSIFIERS WERE TRAINED USING VARIOUS FIXED NUMBERS OF FEATURES (#SELECTED), AS WELL USING ALL FEATURES AVAILABLE (#ALL) AND A VARYING NUMBER SELECTED USING NESTED CROSS-VALIDATION INSIDE THE TRAINING SET (#NESTED).

#ROIs	#pairs	#selected total #features	10	25	50	100	250	500	1000	1500	2000	2500	3000	all	**#nested**
116	6670	4073	0.70	0.69	0.72	0.73	0.81	0.82	0.83	0.82	0.81	0.80	0.75	0.70	**0.80**
639	203841	125967	0.71	0.81	0.81	0.81	0.84	0.87	0.88	0.90	0.90	0.90	0.90	0.77	**0.86**

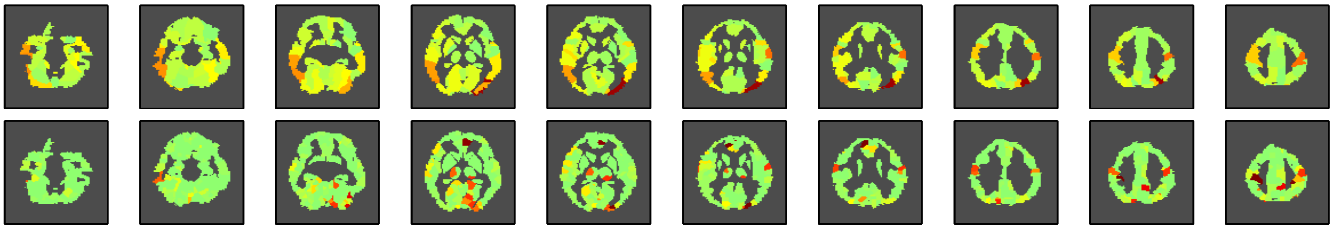

Figure 4. **top:** ROI impact maps using AAL atlas **bottom:** ROI impact maps using the atlas produced with our method

was gauged by multiplying its linear SVM weight for the correct class prediction in the test examples in each fold, and averaging across examples. We then averaged feature impact across the 30 samplings described above. Given that each feature corresponds to a pair of ROIs, we calculated the impact of a ROI by summing the impact across all features corresponding to pairs involving that ROI. We then normalized the ROI impact vector to add up to 1.

Table II shows the top 10 ROIs with the highest impact for AAL and AALsub. Figure 4 shows the voxels in each ROI colored by their impact values. Note how the AALsub map is far sparser than that for AAL, and how high impact values in AAL ROIs can become localized to small parcels of those ROIs; the maps coincide well around the central sulcus, in particular.

V. CONCLUSIONS

Our results indicate that our method produces an atlas subdivision that leads to cleaner functional connectivity features, in the sense that they are both sparser and more informative than the ones based on the original atlas. This translates into being able to narrow down informative locations more precisely; the fact that somato-motor regions have high impact makes sense given the significant alterations seen in these regions both during exogenous processing and endogenous processing in MS patients [11].

REFERENCES

[1] J. Richiardi, M. Gschwind, S. Simioni, J.-M. Annoni, B. Greco, P. Hagmann, M. Schluep, P. Vuilleumier, and D. Van De Ville, "Classifying minimally-disabled multiple sclerosis patients from resting-state functional connectivity," *NeuroImage*, 2012.

[2] J. Bohland, S. Saperstein, F. Pereira, J. Rapin, and L. Grady, "Network, anatomical, and non-imaging measures for the prediction of adhd diagnosis in individual subjects," *Frontiers in Systems Neuroscience*, vol. 6, 2012.

[3] R. Craddock, G. James, P. Holtzheimer III, X. Hu, and H. Mayberg, "A whole brain fmri atlas generated via spatially constrained spectral clustering," *Human brain mapping*, 2011.

[4] T. Blumensath, T. E. Behrens, and S. M. Smith, "Resting-state fmri single subject cortical parcellation based on region growing," in *Medical Image Computing and Computer-Assisted Intervention–MICCAI 2012*. Springer, 2012, pp. 188–195.

[5] V. Blondel, J. Guillaume, R. Lambiotte, and E. Lefebvre, "Fast unfolding of communities in large networks," *Journal of Statistical Mechanics: Theory and Experiment*, no. 10, pp. 1–12, 2008. [Online]. Available: http://iopscience.iop.org/1742-5468/2008/10/P10008

[6] S. Smith, M. Jenkinson, M. Woolrich, C. Beckmann, T. Behrens, H. Johansen-Berg, P. Bannister, M. De Luca, I. Drobnjak, D. Flitney, R. Niazy, J. Saunders, J. Vickers, Y. Zhang, N. De Stefano, and P. Brady, J.M. amd Matthews, "Advances in functional and structural MR image analysis and implementation as FSL." *NeuroImage*, vol. 23, pp. 208–219, 2004.

[7] N. Tzourio-Mazoyer, B. Landeau, D. Papathanassiou, F. Crivello, O. Etard, N. Delcroix, B. Mazoyer, and M. Joliot, "Automated anatomical labeling of activations in SPM using a macroscopic anatomical parcellation of the mni mri single-subject brain," *Neuroimage*, vol. 15, no. 1, pp. 273–289, Jan 2002. [Online]. Available: http://www.hubmed.org/display.cgi?uids=11771995

[8] C. R. Genovese, N. A. Lazar, and T. Nichols, "Thresholding of statistical maps in functional neuroimaging using the false discovery rate," *Neuroimage*, vol. 15, no. 4, pp. 870–878, 2002.

[9] C.-C. Chang and C.-J. Lin, *LIBSVM: A library for support vector machines*, National Taiwan University, 2001.

[10] F. Pereira, T. Mitchell, and M. Botvinick, "Machine learning classifiers and fmri: a tutorial overview," *Neuroimage*, vol. 45, no. 1 Suppl, p. S199, 2009.

[11] A. Janssen, B. Patterson, A. Boster, A. Abduljalil, and R. Prakash, "Altered patterns of neural connectivity are associated with cognitive performance and disease severity in relapsing-remitting multiple sclerosis," (in review).